Journal of Mechanical Engineering and Sciences (JMES)
ISSN (Print): 2289-4659; e-ISSN: 2231-8380; Volume 2, pp. 206-216, June 2012

DOI: http://dx.doi.org/10.15282/jmes.2.2012.8.0019

STEADY STATE VORTEX STRUCTURE OF LID DRIVEN FLOW INSIDE SHALLOW SEMI-ELLIPSE CAVITY

M.S. Idris[1], M.A.M. Irwan[2] and N.M.M. Ammar[1]

[1]Computational Analysis Group,
Faculty of Mechanical Engineering,
Universiti Malaysia Pahang (UMP), 26600 Pekan, Pahang, Malaysia
Email: idriss@ump.edu.my
[2]Faculty of Mechanical Engineering,
Universiti Teknikal Malaysia Melaka (UTeM), 76100,
Durian Tunggal, Melaka, Malaysia

ABSTRACT

In this paper, the lid driven cavity flow inside a semi-ellipse shallow cavity was simulated using the stream function vorticity approach emphasising the non-uniform grid method. Three aspect ratios of 1:4, 1:3 and 3:8 were simulated using laminar flow conditions (range of Reynolds numbers of 100–2000). Primary and secondary vortexes were monitored extensively through centre vortex location, streamlines pattern and peak stream function values. Secondary vortexes developed at Re 1500 for the aspect ratio of 1:4, whereas secondary vortexes formed at an earlier Reynolds number of 1000 for the aspect ratios of 1:3 and 3:8. The size of secondary vortexes increases as the Reynolds number increases. Similar trends can be observed in the differences between primary vortex separation angle and reattachment angle. For the entire streamline pattern, many primary vortex centre locations were situated at the right side of the cavity.

***Keywords*:** Semi-ellipse, lid driven cavity flow, DNS, non-uniform.

INTRODUCTION

Lid driven cavity flow is one of the well-known fluid problems that is solved numerically and considered by many as an attractive and seductive problem. The latter consideration is quite because of the lid driven cavity flow not depleting over the years. There are many uses of the lid driven cavity flow solution in powder technology, mixing, segregating and the formation of eddies (Kosinski, Kosinska, & Hoffmann, 2009). This is due to the mathematical part and the fluid physics contained within the problem itself. Nonetheless, the lid driven cavity flow solution was prepared by Ghia, Ghia, and Shin (1982). Other papers (Barragy & Carey, 1997, Botella & Peyret, 1998) have embarked upon a new paradigm for the lid driven cavity flow solution. However, many researchers focus on the numerical solution to top driven lid square cavity flow, which reflects the mathematical part. For instance, the lid driven cavity flow of a square cavity with top lid moving can be solved using: the finite difference method (Weinan & Liu, 1996), the finite volume method (Perić, Kessler, & Scheuerer, 1988), the Lattice Boltzmann method (Azwadi & Idris, 2010; Zin & Sidik, 2010), the Chebyshev projection method (Botella, 1997) and the spectral method. There are other types, such as the two driven side (Albensoeder, Kuhlmann, & Rath, 2001) and even four sided driven boundary (Wahba, 2009), while others study the effects of shallow cavity (Zdanski, Ortega, & Fico Jr, 2003), deep cavity (Cheng & Hung, 2006) and vorticity

boundary conditions (Weinan & Liu, 1996). These research studies only focused on a rectangular cavity. Several scientists freed themselves from adhering to studies of a rectangular cavity and instead investigated a triangular cavity (Li & Tang, 1996, Ribbens, 1994, Jyotsna &Vanka, 1995, Erturk & Gokcol, 2007), a trapezoidal cavity (McQuain, Ribbens, Wang, & Watson, 1994; Zhang et al., 2010) and semi-circular cavity (Mercan & Atalik, 2009, Chang & Cheng, 1999, Cheng & Chen, 2005). There are also real experiments on lid driven cavity flow (Koseff & Street, 1984a; Koseff & Street, 1984b; Prasad & Koseff, 1989). According to the authors' review of the literature, there is little information regarding lid driven cavity flow inside a semi-elliptical boundary due to the complexity of the boundary. Therefore, this research will be conducted to provide the physical fluid behaviour and numerical results of lid driven cavity flow inside a shallow semi-ellipse cavity. The aspect ratio is chosen rather than eccentricity because of the inability of eccentricity to distinguish between shallow or deep semi-ellipses. There are three aspect ratios used for the simulation, which are 1:4, 1:3 and 3:8. An aspect ratio of 1:2 is not considered because this value is equivalent to a semi-circular cavity. For each aspect ratio, five Reynolds numbers (Re) of 100, 500, 1000, 1500 and 2000 are simulated to monitor the behaviour of vortexes, vortex centre location value and stream function peak values, as well as separation angles.

GOVERNING EQUATIONS AND NUMERICAL FORMULATION

This study was conducted with emphasis on the stream function vorticity approach. For this research, there are several main equations with a few auxiliary equations. These main equations are the vorticity transport equation (1) and the vorticity equation in terms of stream function (2). These equations are in dimensionless form and all parameters are independent.

$$\frac{\partial \Omega}{\partial T} + U\frac{\partial \Omega}{\partial X} + V\frac{\partial \Omega}{\partial Y} = \frac{1}{Re}\left(\frac{\partial^2 \Omega}{\partial X^2} + \frac{\partial^2 \Omega}{\partial Y^2}\right) \tag{1}$$

$$\frac{\partial^2 \Psi}{\partial X^2} + \frac{\partial^2 \Psi}{\partial Y^2} = -\Omega \tag{2}$$

As for the discretisation method, an explicit first order upwind scheme for the temporal derivative and a central finite difference for the spatial derivative of a non-uniform grid were utilised in order to obtain the numerical simulation. A special formulation for the spatial derivative is implemented to mimic the curvilinear shape of the elliptical boundary. The special formulation was introduced and the formulation of the first and second order derivatives of a non-uniform spatial grid approximation was proven more effective than previous non-uniform grid equations, those were implemented and are represented by Eqs (3 & 4) (Veldman & Rinzema, 1992) and for the physical formulation, the collocated nodes of the non-uniform grid size are presented in Figure 1.

$$\frac{\partial f}{\partial x} \cong \frac{f(x_{i+1}) - f(x_{i-1})}{h_a + h_b} \tag{3}$$

$$\frac{\partial^2 f}{\partial x^2} \cong \frac{2f(x_{i+1})}{h_a(h_b + h_a)} - \frac{2}{h_a h_b} f(x_i) + \frac{2f(x_{i-1})}{h_b(h_b + h_a)} \tag{4}$$

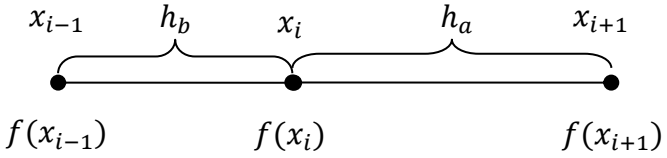

Figure 1. One dimensional non-uniform grid.

BOUNDARY DISCRETISATION

The boundary of a semi-ellipse cavity is crucial, especially at the bottom part with a grid 14 × 7, as shown in Figure 2. When the grid spacing of an actual 128 × 128 grid is to be presented as the cavity model, the special spacing arrangement is difficult display. For the model of a semi-elliptic cavity the mesh is unique, whereas the grid spacing is different. The spacing needs to be implemented to facilitate the curved shape of the bottom cavity, which adopts the curvature of an isosceles triangle cavity. According to Figure 2, the length of the lid, *L* (top boundary) is maintained at unity, whilst the cavity height (*H*) changes for the various shallow aspect ratios (H/L or AR) of 1:4, 1:3 and 3:8. Hence, the irregular spacing of the grid should compensate for the non-uniform equation for the derivatives terms.

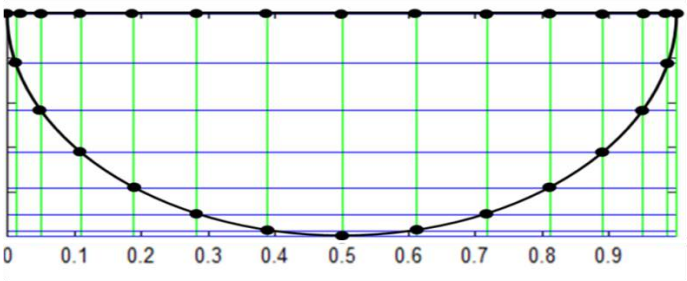

Figure 2. Semi-ellipse cavity model.

RESULTS AND DISCUSSION

The grid independent tests were performed for 30 × 30, 60 × 60, 100 × 100 and 128 × 128. The obtained results indicate a satisfactory result of streamlines pattern, location of primary and secondary vortex centres, together with the value of peak stream function at grid value of 60 × 60. However, the 128 × 128 grid was selected for use for better accuracy, although at the expense of time. Figure 3 shows the streamlines pattern on the left and the vorticity contour on the right. This aspect ratio resembled the depth of a semi-ellipse cavity ratio to length of lid. For Re < 1500, the secondary vortex is absent, which leaves the primary vortex alone. Nevertheless, the centre of the primary vortex changes from the centre of the cavity to the left of the cavity as the Reynolds number increases. Table 1 presents the location of centre vortex and stream function value, for both the primary and secondary vortex for an aspect ratio of 1:4. The change of location of the vortex centre is significant in the horizontal direction with values of 0.5490, 0.7357 and 0.7464. However, there are only small changes in the location of the primary

vortex centre in the vertical direction with values of 0.8420, 0.8420 and 0.9000. Meanwhile, for Re 1500 and 2000, a secondary vortex was developed with centre locations of (0.5123, –0.1933) and (0.5123, –0.1723). The peak values of stream function are 0.00096 and 0.00213. On the other hand, the stream function value of the primary vortex, together with each location for Re 1500 and 2000 are –0.03983 at (0.7674, 0.0900) and –0.03858 at (0.7879, 0.0842). It can be seen that the pattern is visible when the size of the secondary vortex increases as the Reynolds number increases. Both secondary vortexes are attached to the middle of the curvilinear boundary.

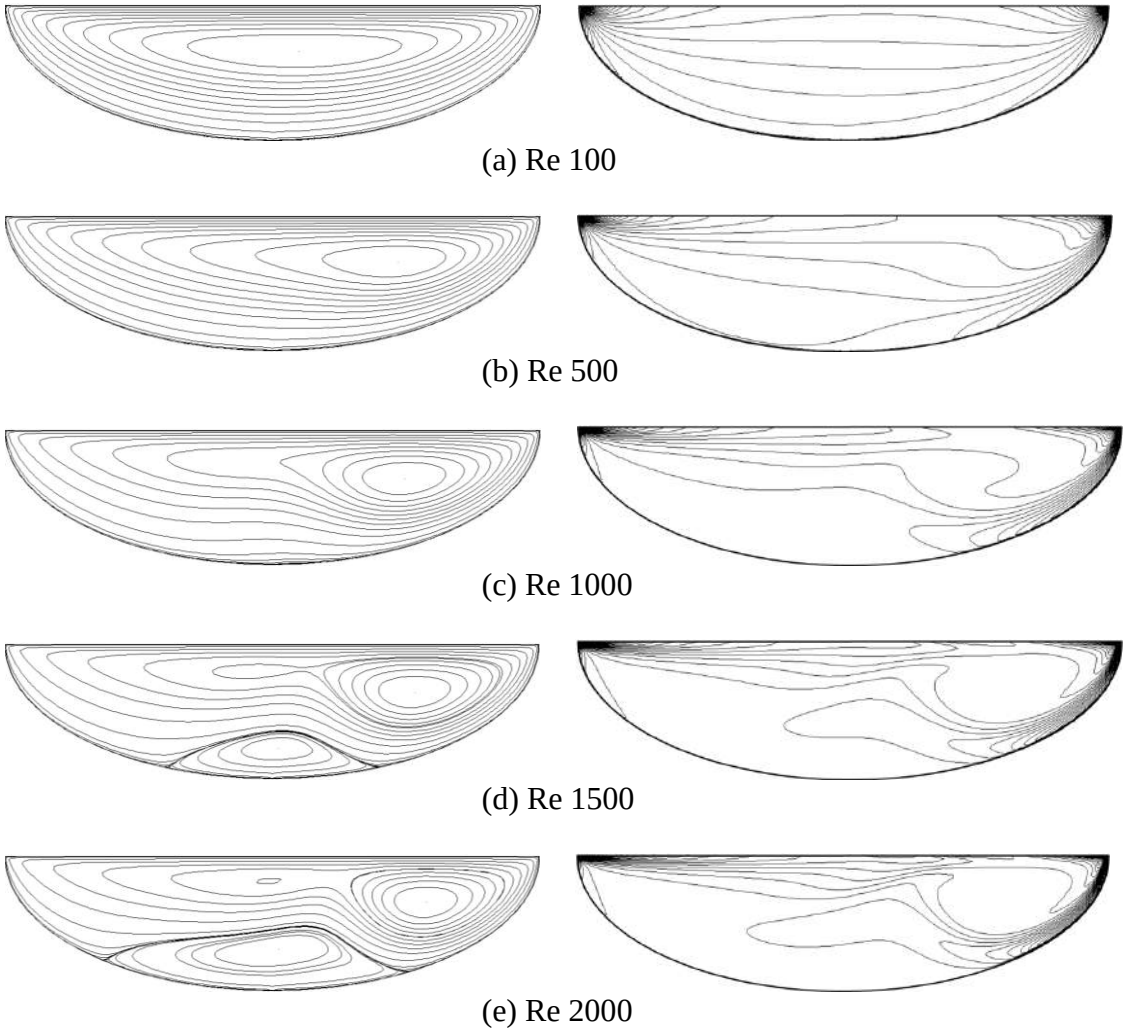

(a) Re 100

(b) Re 500

(c) Re 1000

(d) Re 1500

(e) Re 2000

Figure 3. Streamlines pattern and vorticity contour for semi ellipse with aspect ratio of 1:4 for various Reynolds numbers.

The condition of secondary vortex attachment and separation towards the curvilinear body is extracted from the simulation results. The sketch of the angles is shown in Figure 4. The angles are calculated counter-clockwise from the left side of cavity to the right side of cavity, where θ_1 represents the attachment angle of the secondary vortex towards the curvilinear boundary and θ_2 represents the angle of separation of the secondary vortex from the curvilinear boundary. These angles of

attachment and separation are then compiled inside Table 2. It can be seen that the secondary vortex is attached at an angle of 48.442º and is detached from the curvilinear boundary at an angle of 131.55º for Re of 1500. Meanwhile, for Re of 2000, the secondary vortex is attached at an earlier angle of 31.352º and it separates from the curvilinear boundary at an angle of 140.165º. These angles are influenced by the size of the secondary vortex itself. It can be observed that for the secondary vortex, the attachment angle decreases and the separation angle increases as the Reynolds number increases. For the vorticity contour, significant changes can be observed at the right side of the cavity as the centre of the primary vortex becomes located around this area.

Table 1. The primary and secondary vortex centre location and stream function values for aspect ratio of 1:4 with various Reynolds numbers.

Re	Primary vortex centre location	Stream function value, Ψ	Secondary vortex centre location	Stream function value, Ψ
100	(0.5490, 0.0842)	–0.03650	-	-
500	(0.7357, 0.0842)	–0.03803	-	-
1000	(0.7464, 0.0900)	–0.04055	-	-
1500	(0.7674, 0.0900)	–0.03983	(0.5123, –0.1933)	0.00096
2000	(0.7879, 0.0842)	–0.03858	(0.5123, –0.1723)	0.00213

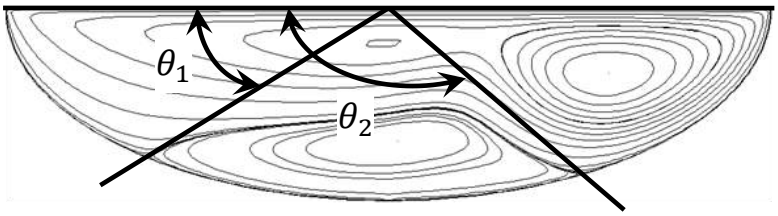

Figure 4. The angle of the separation and reattachment points.

Table 2. Angles of separation and reattachment of secondary vortex for aspect ratio 1:4 (in degrees).

Re	θ_1	θ_2
1500	48.442	131.558
2000	31.352	140.165

The streamlines pattern and vorticity contours are displayed in Figure 5. The simulation conditions and parameters remained the same with an aspect ratio of 2:3. It can be observed that the secondary vortex develops at an earlier value of the Reynolds number (1000) and that the secondary vortex only appears for a Reynolds number of 1500. It can be noted that as the Reynolds number increases, the size of the secondary vortex also increases. This condition is obvious for Reynolds numbers of 1000 and higher. The primary and secondary vortex centre locations and stream function values for the aspect ratio 1:3 with various Reynolds numbers are listed in Table 3. The primary vortex centre location shows obvious changes as the horizontal value moved to

the left of the cavity as the Reynolds number increases, whereas for the vertical value, most of the values settled at 0.1200 below the moving boundary. For the stream function, for Reynolds numbers 100 and 500, the value seems to be increasing. However, for Reynolds numbers 1000, 1500 and 2000, the stream function magnitude decreases from −0.05291 to −0.05005 due to the appearance and the size of the secondary vortex, which counters the primary vortex. On the other hand, the stream function value at the peak increased from 0.00082 to 0.00505 for the secondary vortex when the Reynolds number increased from 1000 to 2000. As for the location of the secondary vortex centre, it moves steadily downwards in the cavity when the Reynolds number increases.

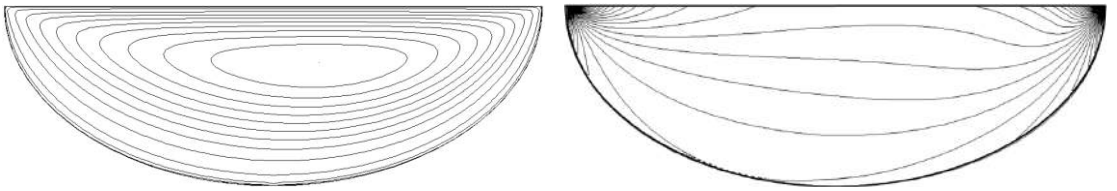

(a) Re 100

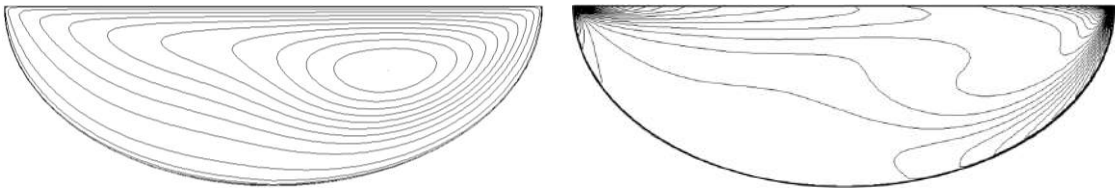

(b) Re 500

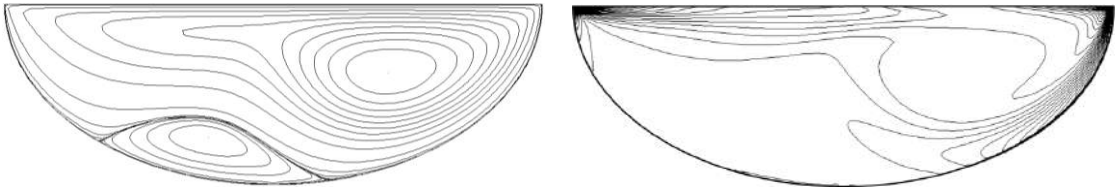

(c) Re 1000

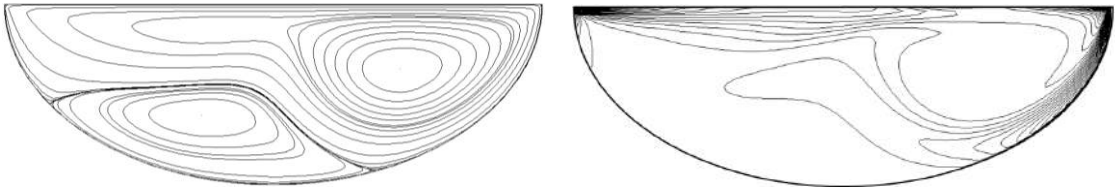

(d) Re 1500

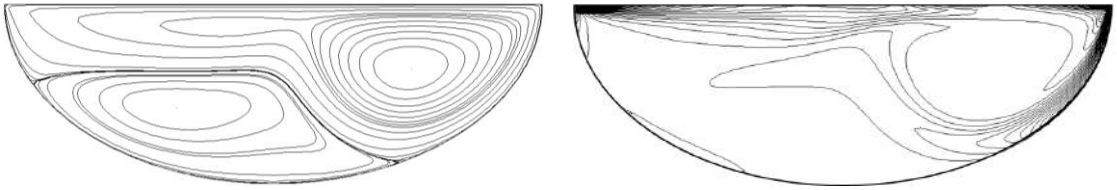

(e) Re 2000

Figure 5. Streamlines pattern and vorticity contour for semi ellipse with aspect ratio of 1:3 for various Reynolds number.

Table 3. The primary and secondary vortex centre locations and stream function values for aspect ratio 1:3 with various Reynolds numbers.

Re	Primary vortex centre location	Stream function value, Ψ	Secondary vortex centre location	Stream function value, Ψ
100	(0.5855, –0.2288)	–0.04811	-	-
500	(0.7138, –0.1200)	–0.05257	-	-
1000	(0.7138, –0.1276)	–0.05291	(0.3786, –0.0864)	0.00082
1500	(0.7357, –0.1200)	–0.05133	(0.3666, –0.2051)	0.00301
2000	(0.7571, –0.1200)	–0.05005	(0.3201, –0.1919)	0.00505

Table 4 shows the angle of separation and attachment for the secondary vortex with the aspect ratio 1:3. The presence of the secondary vortex is greater than previous parts of the simulation. It is obvious that the attachment angle for the secondary vortex decreases from 37.699º to 18.550º and that the separation angle increases from 108.615º to 128.721º when the Reynolds number increases from 1000 to 2000. This result is similar to the streamlines pattern result, which shows that the size of the secondary vortex increases as the Reynolds number increases. The difference between θ_1 and θ_2 is 70.916º, 97.843 and 110.171º for a Reynolds number of 1000, 1500 and 2000, respectively. It is obvious that an increasing difference of θ_1 causes the secondary vortex to become larger.

Table 4. Angles of separation and reattachment of secondary vortex (in degrees) for aspect ratio of 1:3.

Re	θ_1	θ_2
1000	37.699	108.615
1500	24.011	121.854
2000	18.550	128.721

Meanwhile, for an aspect ratio of 3:8, the streamlines pattern and vorticity contour are presented in Figure 6. It can be observed that no secondary vortex developed inside the cavity at Reynolds numbers of 100 and 500. A secondary vortex only appeared when the Reynolds number increased to 1000 and higher. Regarding the value of stream function, the magnitudes increased from –0.05376 to –0.05888 when the Reynolds number increased from 100 to 500. The magnitudes of the stream function decreased from –0.05874 to –0.05538 when the Reynolds number increased from 1000 to 2000. This phenomenon is mostly due to the occurrence of the secondary vortex rotation, which rotates counter to the primary vortex rotating direction. Therefore, the secondary vortex acts as an obstacle to the primary vortex, reducing the value of the peak stream function even though the Reynolds number is rising. For the vorticity contour, the significant changes can be observed at the right sight of the cavity where the centre of the primary vortex is located. The stream function peak value and its location for both the secondary and primary vortexes are provided in Table 5.

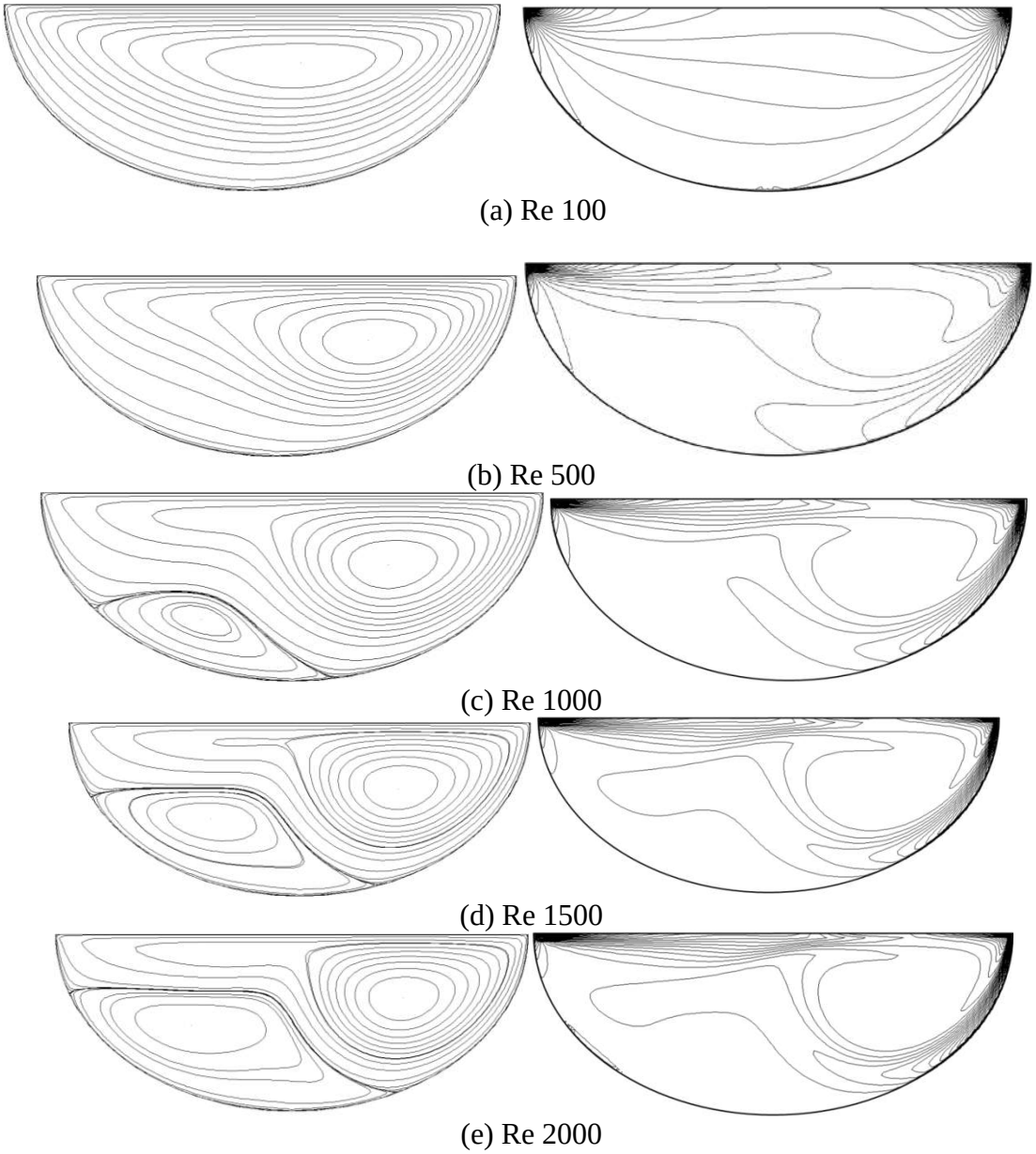

(a) Re 100

(b) Re 500

(c) Re 1000

(d) Re 1500

(e) Re 2000

Figure 6. Streamlines pattern and vorticity contour for semi-ellipse with aspect ratio of 3:8 for Re 100, 500, 1000, 1500 and 2000.

Table 5. The primary and secondary vortex centre locations and stream function values for aspect ratio of 3:8 with various Reynolds numbers.

Re	Primary vortex centre location	Stream function value, Ψ	Secondary vortex centre location	Stream function value, Ψ
100	(0.5975, –0.1176)	–0.05376	-	-
500	(0.6913, –0.1350)	–0.05888	-	-
1000	(0.6913, –0.1435)	–0.05874	(0.3201, –0.2518)	0.00126
1500	(0.7138, –0.1435)	–0.05716	(0.3087, –0.2083)	0.00379
2000	(0.7357, –0.1350)	–0.05538	(0.2862, –0.1928)	0.00505

The angle of separation and reattachment of the secondary vortex for an aspect ratio of 3:8 or 3:4 of the half-ellipse are presented in Table 6. Similar to the aspect ratio 3:4, the secondary vortex starts to appear inside the cavity at Re number 1000. Initially, the primary vortex separates from the boundary at an angle of 30.341º and then reattaches to the curvilinear boundary when the angle reaches 103.264º. The primary vortex separates earlier at an angle of 19.531º and reattaches at later angle of 115.505º for a Reynolds number of 1500. The primary vortex separates at an angle of 15.022º for a Reynolds number of 2000 and reattaches at an angle of 123.867º, which is greater than for a Reynolds number of 1500. The difference between the separation angle and reattachment angle increases as the Reynolds number increases.

Table 6. Angles of separation and reattachment of secondary vortex (in degrees).

Re	θ_1	θ_2
1000	30.341	103.264
1500	19.531	115.505
2000	15.022	123.867

CONCLUSIONS

The lid driven cavity flow inside a semi-ellipse shallow cavity was simulated for different aspect ratios and Reynolds numbers. The primary and secondary vortex behaviour was observed, together with the vortex centre location and magnitude of the peak stream function value. The angle of separation and reattachment for the primary and secondary vortexes were obtained when the secondary vortex developed. It can be seen that as the Reynolds number increases to an average of 1000 for every aspect ratio, the secondary vortex developed in the cavity. As the Reynolds number increases, the size of the secondary vortex also increases. The increment depth of the cavity also played an important part in the relationship between the Reynolds number and the secondary vortex. The non-uniform finite difference method has been demonstrated to be successful for simulating the non-square finite difference problem.

ACKNOWLEDGEMENTS

The authors would like to thank Universiti Malaysia Pahang for provides laboratory facilities and financial support under project no. RDU110382.

REFERENCES

Albensoeder, S., Kuhlmann, H. C., & Rath, H. J. (2001). Multiplicity of steady two-dimensional flows in two-sided lid-driven cavities. *Theoretical and Computational Fluid Dynamics*, 14, 223-241.

Azwadi, C. S. N., & Idris, M. S. (2010). Finite different and lattice boltzmann modelling for simulation of natural convection in a square cavity. *International Journal of Mechanical and Materials Engineering*, 5, 80-86.

Barragy, E., & Carey, G. F. (1997). Stream function-vorticity driven cavity solution using P finite elements. *Computers and Fluids*, 26, 453-468.

Botella, O. (1997). On The solution of the Navier-stokes equations using Chebyshev projection schemes with third-order accuracy in time. *Computers and Fluids*, 26, 107-116.

Botella, O., & Peyret, R. (1998). Benchmark spectral results on the lid-driven cavity flow. *Computers and Fluids*, 27, 421-433.

Chang, M. H., & Cheng, C. H. (1999). Predictions of lid-driven flow and heat convection in an arc-shape cavity. *International Communications in Heat and Mass Transfer*, 26, 829-838.

Cheng, C. H., & Chen, C. L. (2005). Buoyancy-induced periodic flow and heat transfer in lid-driven cavities with different cross-sectional shapes. *International Communications in Heat and Mass Transfer*, 32, 483-490.

Cheng, M., & Hung, K. C. (2006). Vortex structure of steady flow in a rectangular cavity. *Computers and Fluids*, 35, 1046-1062.

Erturk, E., & Gokcol, O. (2007). Fine grid numerical solutions of triangular cavity flow. *Epj Applied Physics*, 38, 97-105.

Ghia, U., Ghia, K. N., & Shin, C. T. (1982). High-Re Solutions for incompressible flow using the Navier-stokes equations and a multigrid method. *Journal of Computational Physics*, 48, 387-411.

Jyotsna, R., & Vanka, S. P. (1995). Multigrid calculation of steady, viscous flow in a triangular cavity. J*ournal of Computational Physics*, 122, 107-117.

Koseff, J. R., & Street, R. L. (1984a). On end wall effects in a lid-driven cavity flow. *Journal of Fluids Engineering, Transactions of The ASME*, 106, 385-389.

Koseff, J. R., & Street, R. L. (1984b). Visualization studies of a shear driven three-dimensional recirculating flow. *Journal of Fluids Engineering, Transactions of The ASME*, 106, 21-29.

Kosinski, P., Kosinska, A., & Hoffmann, A. C. (2009). Simulation of solid particles behaviour in a driven cavity flow. *Powder Technology*, 191, 327-339.

Li, M., & Tang, T. (1996). Steady viscous flow in a triangular cavity by efficient numerical techniques. *Computers and Mathematics with Applications*, 31, 55-65.

McQuain, W. D., Ribbens, C. J., Wang, C. Y., & Watson, L. T. (1994). Steady viscous flow in a trapezoidal cavity. *Computers and Fluids*, 23, 613-626.

Mercan, H., & Atalik, K. (2009). Vortex Formation in lid-driven arc-shape cavity flows at high reynolds numbers. *European Journal of Mechanics, B/Fluids*, 28, 61-71.

Perić, M., Kessler, R., & Scheuerer, G. (1988). Comparison of finite-volume numerical methods with staggered and colocated grids. *Computers and Fluids*, 16, 389-403.

Prasad, A. K., & Koseff, J. R. (1989). Reynolds number and end-wall effects on a lid-driven cavity flow. *Physics of Fluids A*, 1, 208-218.

Ribbens, C. J. (1994). Steady viscous flow in a triangular cavity. *Journal of Computational Physics*, 112, 173-181.

Veldman, A. E. P., & Rinzema, K. (1992). Playing with nonuniform grids. *Journal of Engineering Mathematics*, 26, 119-130.

Wahba, E. M. (2009). Multiplicity of states for two-sided and four-sided lid driven cavity flows. *Computers and Fluids*, 38, 247-253.

Weinan, E., & Liu, J. G. (1996). Vorticity boundary condition and related issues for finite difference schemes. *Journal of Computational Physics*, 124, 368-382.

Zdanski, P. S. B., Ortega, M. A., & Fico Jr, N. G. C. R. (2003). Numerical study of the flow over shallow cavities. *Computers and Fluids*, 32, 953-974.

Zhang, T., Shi, B., & Chai, Z. (2010). Lattice Boltzmann simulation of lid-driven flow in trapezoidal cavities. *Computers and Fluids*, 39, 1977-1989.

Zin, M. R. M., & Sidik, N. A. C. 2010. An accurate numerical method to predict fluid flow in a shear driven cavity. *International Review of Mechanical Engineering*, 4, 719-725.